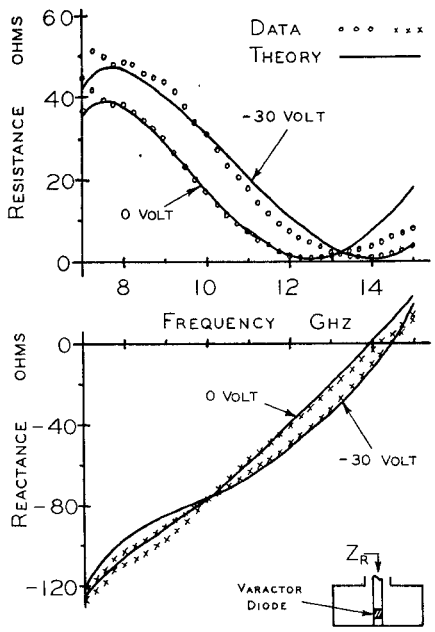


Fig. 9. Theory and experimental comparison for varactor tuning.

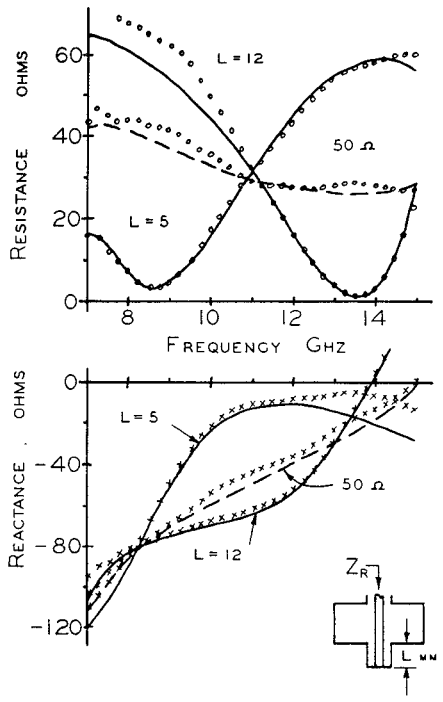


Fig. 10. Theory and experimental comparison for a 50-Ω load and a sliding short.

varactor model was used as the gap load with $L_s = 0.45$ nH, $C_p = 0.2$ pF, $R_s = 0.95\,\Omega$, $C_j(0v) = 1.9$ pF, and $C_j(-30v) = 0.45$ pF. (Note the interesting effect at midband (10 GHz) where the reactance stays constant but the real part shifts from 17 to 31 Ω. This would be more useful for amplitude modulation than for frequency tuning of a Gunn diode.)

The next mount example shown in Fig. 10 uses the double coax configuration, requiring an equivalent gap representation at both ports. Three different loading conditions are established at $Z_{G2}$ to demonstrate the versatility of this configuration. First a 50-Ω coaxial match is used to represent a lossy load. Then two different positions of a sliding short are used to represent widely varying reactive loading. The correlation between the measured data and the theory is excellent for all three conditions. 25- and 100-Ω loads were also measured along with many other short positions. The examples shown, however, were chosen as typical and do not represent best cases.

## IV. Summary and Conclusions

An equivalent circuit for a 2-gap waveguide mount has been presented. Also, an equivalence has been demonstrated between a coaxial entry and an equivalent gap for this type mount. Using this information, theoretical curves for various configurations were generated and compared with measured data. Excellent correlation was observed, indicating the accuracy of the equivalent circuit modeling for use in microwave component design.

## References

[1] M. Dean and M. J. Howes, "An electronically tuned Gunn oscillator circuit," *IEEE Trans. Electron Devices*, vol. ED-20, no. 6, pp. 597–598, June 1973.
[2] R. L. Eisenhart, P. T. Greiling, L. K. Roberts, and R. Robertson, "A useful equivalence for a coaxial-waveguide junction," to be published.
[3] N. D. Kenyon, "A circuit design of millimeter-wave IMPATT oscillators," *IEEE Microwave Symposium Digest*, Newport Beach, CA, May 1970.
[4] R. L. Eisenhart and P. J. Khan, "Theoretical and experimental analysis of a waveguide mounting structure," *IEEE Trans. Microwave Theory Tech.*, vol. MTT-19, pp. 706–719, August 1971.
[5] R. E. Collin, *Foundations for Microwave Engineering.* McGraw-Hill, 1966, p. 164.
[6] L. Lewin, "A contribution to the theory of probes in waveguides," *Proc. Inst. Elec. Eng.*, Monogr. 259R, pp. 109–116, Oct. 1957.

# An Improved Solid-State Noise Source

MOTOHISA KANDA

***Abstract*—An improved solid-state noise source is discussed. By implementing such modifications as 1) heat sinking of a silicon avalanche noise diode, 2) proper dc RF decoupling, and 3) impedance matching, the stability of the National Bureau of Standards (NBS) solid-state noise source is improved significantly over that of typical commercial solid-state noise sources. These modifications, how they are implemented, and the resulting improvement in stability are described.**

## I. Introduction

The convenience of a high-level noise output with a potential for fast switching makes a solid-state noise source ideal for system noise monitor applications. However, solid-state noise sources are relatively easily influenced by their environment, and an unsuitable environment can cause unstable operation.

A preliminary study on the stability of typical commercial solid-state noise sources indicated that the fluctuations of the output noise for a typical commercial solid-state noise source exhibit a random walk noise behavior (which is divergent toward lower frequencies) in its average noise output. The square root of the variance of the average output noise power for a one-day sampling time interval is typically 0.008 dB [1], [2]. The low frequency divergent instability is attributed to the noise diode itself and to the external circuit in which it is used. The stability of a solid-state noise source can be improved by properly

Manuscript received March 31, 1976; revised July 22, 1976.
The author is with the Electromagnetics Division, National Bureau of Standards, Boulder, CO 80302.

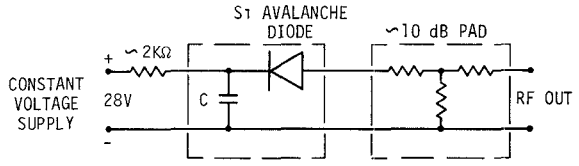


Fig. 1. Schematic diagram for a typical commercial solid-state noise source.

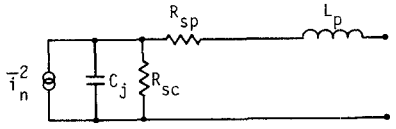


| $V_{breakdown}$ | $C_j(-5V)$ | $R_s$ | $R_{sc}$ | $R_{sp}$ | $L_p$ |
|---|---|---|---|---|---|
| 8.2 V | 1.2 pF | ~14Ω | ~12Ω | ~2Ω | ~1.5 nH |

Fig. 2. Equivalent circuit of a silicon avalanche noise diode.

mounting the noise diode with adequate consideration being given to both dc and RF decoupling and to impedance matching.

The purpose of this short paper is to describe one way by which to improve the stability of a solid-state noise source. A schematic diagram for a typical commercial solid-state noise source is shown in Fig. 1. There are three areas that can be modified to improve its stability, namely, 1) heat sinking of the noise diode, 2) proper dc and RF decoupling, and 3) impedance matching. These modifications significantly improve the stability of the National Bureau of Standards (NBS) solid-state noise source over that of a typical commercial solid-state noise source.

## II. Noise Diode Characteristics

Generally, a silicon avalanche diode is suitable for use as a noise diode. The characterization of silicon avalanche diodes has been studied considerably [3], [4]. The purpose of this section is to describe typical characteristics of the silicon avalanche diode which can be used for the solid-state noise source.

Commercially available silicon avalanche noise diodes revealed large variations from diode to diode, and the breakdown voltage of these diodes lies typically between 8 and 12 V. A semiconductor p-n junction under reverse bias can be modeled by a combination of a depletion layer capacitance $C_j$, a space-charge resistance $R_{sc}$ [5], a spreading resistance $R_{sp}$ [5], and a lead inductance $L_p$. The equivalent circuit of a silicon avalanche diode is shown in Fig. 2. The value of the depletion layer capacitance, which can be measured at low frequencies, is assumed to be invariant up through the microwave frequencies of interest. The magnitude of the space-charge resistance $R_{sc}$ and the spreading resistance $R_{sp}$ depends strongly on the diameter of the breakdown region. The spreading resistance $R_{sp}$ usually includes the resistance of the gold lead and ohmic contacts as well as the nondepleted region of the silicon substrate.

The total series resistance $R_s$ ($R_s = R_{sc} + R_{sp}$) is readily obtained from the slope of the current–voltage relationship. The experimental results of $R_s$ are plotted as a function of diode currents in Fig. 3. This figure indicates that the series resistance $R_s$ is approximately 14 Ω and is independent of diode current except at a lower current level where the breakdown region decreases, and hence $R_s$ tends to increase.

To estimate the spreading resistance $R_{sp}$ of the avalanche diode, an automated network analyzer was used. By changing the diode bias from a reverse direction to a forward direction,

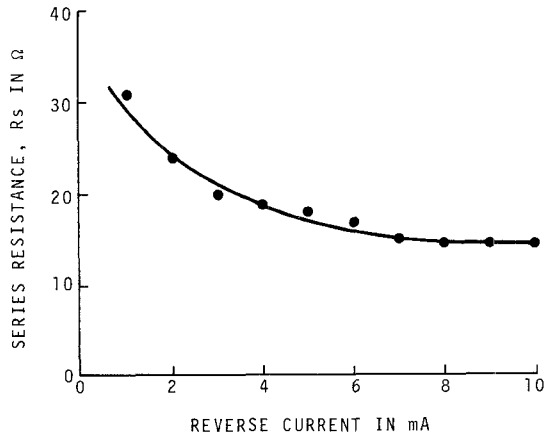


Fig. 3. Diode series resistance as a function of diode current.

the diode impedance display on the Smith chart changes from a constant resistive part ($R_{sp}$) to a constant reactive part ($\omega L_p$). It is found that the spreading resistance $R_{sp}$ of the silicon avalanche diode is approximately 2 Ω and the lead inductance is approximately 1.5 nH. The spreading resistance $R_{sp}$ of 2 Ω was very similar to the calculated value [5]

$$R_{sp} \cong 400 \left(\frac{l_d^2}{A}\right)^{1/2} \cong 2\,\Omega \tag{1}$$

where

$l_d$ width of the drift region $\simeq 5 \times 10^{-7}$ m;
$A$ breakdown area $\simeq 10^{-8}$ m$^2$.

The space-charge resistance $R_{sc}$ is, therefore, estimated to be 12 Ω, which was very similar to the calculated value [5]

$$R_{sc} = \frac{l_d^2}{3\varepsilon v A} \cong 9\,\Omega \tag{2}$$

where

$\varepsilon$ dielectric constant of silicon $\simeq 1 \times 10^{-11}$ F/m;
$v$ maximum drift velocity $\simeq 10^5$ m/s.

The capacitance of the diode was measured by use of an impedance bridge. The junction capacitance was found to follow more closely the $(V + V_b)^{-1/3}$ behavior which is predicted for a graded p-n junction than the $(V + V_b)^{-1/2}$ behavior which is predicted for a step p-n junction. The junction capacitance of approximately 1.2 pF at a reverse-bias voltage $V$ of 5 V with a built-in voltage $V_b$ of approximate 1 V was found, and this junction capacitance was very similar to the calculated value [6]

$$C_j(-V) = \left(\frac{qa\varepsilon^2}{12}\right)^{1/3} (V + V_b)^{-1/3} A \cong 1\text{ pF} \tag{3}$$

where

$q$ electronic charge $\cong 1.6 \times 10^{-19}$ C;
$a$ impurity gradient $\cong 1 \times 10^{31}$/m$^4$;
$V$ reverse voltage across the p-n junction = 5 V;
$V_b$ built-in voltage $\cong$ 1 V.

The characteristics of the silicon avalanche noise diode used are summarized as follows:

| $V_{breakdown}$ | $C_j(-5V)$ | $R_s$ |
|---|---|---|
| 8.2 V | 1.2 pF | ~ 14 Ω |

| $R_{sc}$ | $R_{sp}$ | $L_p$ |
|---|---|---|
| ~ 14 Ω | ~ 2 Ω | ~ 1.5 nH |

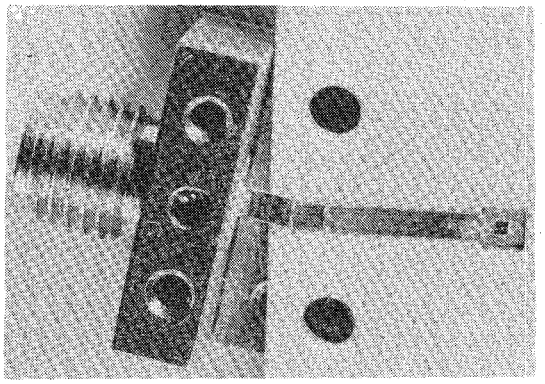

Fig. 4. Compensated 50-Ω stripline with a miniature connector launcher.

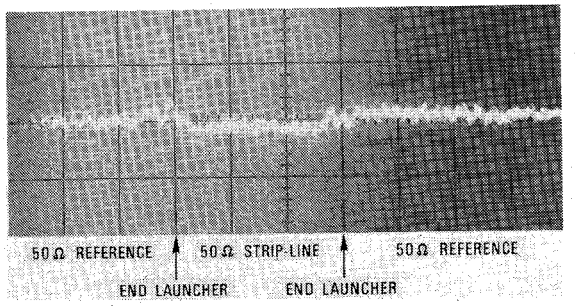


Fig. 5. TDR trace of 50-Ω stripline with a miniature connector launcher. (Vertical: reflection coefficient 0.05/div; Horizontal: 100 ps/div).

Silicon avalanche diodes which exhibit similar characteristics to the preceding are expected to be suitable for use as a noise diode.

## III. Design Features

Several 50-Ω striplines were fabricated. The center strip at the end launcher was trimmed slightly to compensate for the extra capacitance created by the end launcher as shown in Fig. 4. The end launcher has been offset to show the compensated area clearly. The silicon avalanche diode is mounted on the ground plane of the 50-Ω stripline using a gold conductive epoxy. A time-domain-reflectometer (TDR) signature shown in Fig. 5 indicates that the maximum VSWR for this 50-Ω stripline with a miniature connector launcher was 1.04. This configuration incorporates a good heat sinking of the diode active region. A 50-$\mu$m (2-mil) gold wire is bonded to the top of the diode and subsequently to the 50-Ω stripline.

The dc bias input to the diode passes through a low-pass dc stabilization circuit to isolate the power supply from the active device and to prevent any bias interaction. A stripline 3-dB quadrature coupler is used to decouple dc and RF ports neatly. The schematic diagram and the photograph of the NBS solid-state noise source are shown respectively in Figs. 6 and 7.

## IV. Diode Impedance Matching

Changes in the magnitude and/or the phase of the diode impedance can cause unstable operation of a solid-state noise source. Therefore, stable operation of a noise diode requires precise impedance matching of the silicon avalanche diode to its adjoining 50-Ω stripline. The small-signal RF impedance of the diode at 2 GHz was measured in a 50-Ω stripline using an automated network analyzer. The standard calibration program for the network analyzer used incorporates two reference shorts approximately 180° apart at the frequency of interest and a 50-Ω termination.

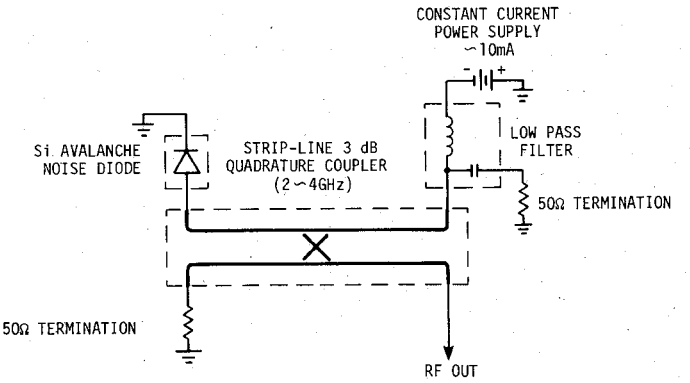


Fig. 6. Schematic diagram of NBS solid-state noise source.

Conventional schemes such as 1) an impedance transformer and 2) an impedance tuner are very useful for providing a good transition from the relatively low diode impedance to the 50-Ω stripline, although these techniques are frequency sensitive and, hence, relatively narrow banded in nature. However, relatively broad-banded matching can be achieved by using two similar diodes mounted onto stripline 3-dB quadrature couplers as shown in Fig. 8. By selecting two diodes with nearly identical impedances (both amplitude and phase), the effect of mismatch from one diode compensates that from the other through the quadrature coupler, and an improvement in the VSWR from 2 to 1.2 was readily achieved at 2 GHz.

Possibly one of the best and perhaps the easiest way to achieve the proper impedance match would be to fabricate one side arm of the stripline 3-dB quadrature coupler with the same impedance as the diode at the operating bias (~ 8 V).

## V. Experimental Technique

A statistical measure of stability applicable to solid-state noise sources is discussed in this section.

### A. A Statistical Measure for the Stability

An important performance parameter for a solid-state noise source is the stability of its mean square output noise as a function of sampling time interval. For some models of noise generation mechanisms which seem to be representative of solid-state noise sources, the classical variance is unbounded. A well-behaved and convergent stability measure is therefore needed. Such has been developed for the field of frequency stability, and the recommended measure for the time-domain frequency stability is an Allan variance [7]–[9]. A special case of an Allan variance analysis [7] is used in this short paper to establish a measure of stability for solid-state noise sources.

A record of the phenomenon under consideration, $y(t)$, is divided into a number of equal time segments of length $\tau$, and the average value of $y(t)$ of each segment $y_k$ is calculated by

$$y_k = \frac{1}{\tau}\int_{t_k}^{t_k+\tau} y(t)\,dt \tag{4}$$

where $y_k$ is the $k$th segment average starting at time $t_k$. Next, the sample variance (sample size two), $\sigma_y^2(2,\tau)$, of successive averages is calculated. That is,

$$\sigma_y^2(2,\tau) = \sum_{n=k}^{k+1}(y_n - \bar{y}_k)^2 = \tfrac{1}{2}(y_{k+1} - y_k)^2 \tag{5}$$

where

$$\bar{y}_k \equiv \frac{1}{2}\sum_{n=k}^{k+1} y_n \tag{6}$$

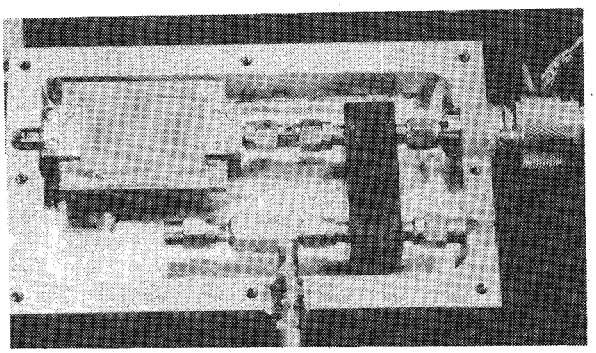

Fig. 7. Photograph of assembled NBS solid-state noise source.

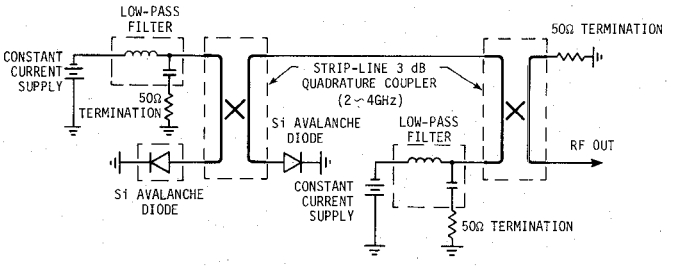


Fig. 8. Broad-band matching technique using two identical noise diodes.

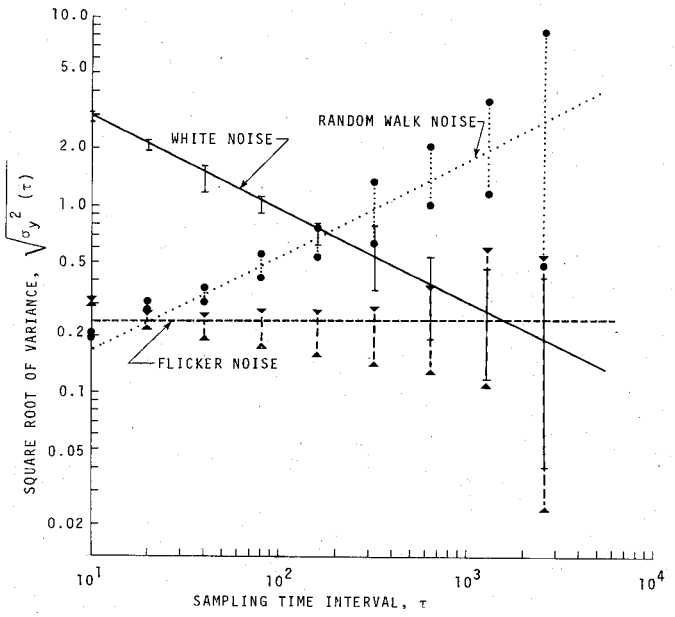


Fig. 9. The square root of Allan variances for three kinds of noise as a function of sampling time interval $\tau$.

is the average of the two successive segment averages $y_k$ and $y_{k+1}$. The Allan variance $\sigma_y^2(\tau)$ for this special case (sample size two) is then defined to be [7]

$$\sigma_y^2(\tau) \equiv \langle \sigma_y^2(2,\tau) \rangle \tag{7}$$

where the brackets represent the infinite time average of $\sigma_y^2(2,\tau)$ over all pairs of successive $y_k$ constructed from $y(t)$. In practice, a finite set of $\sigma_y^2(2,\tau)$ often gives a good estimate of $\sigma_y^2(\tau)$.

The preceding calculation is repeated for various values of sampling time interval $\tau$. For a given maximum allowable rms deviation in $y(t)$, the maximum sampling time interval can then be determined. When the noise generation mechanism is random and unautocorrelated, the Allan variance $\sigma^2(\tau)$ decreases as the inverse of sampling time interval $\tau$. The data analysis is typically performed by a computer via a program designed to compute the appropriate Allan variance. In the computer program logarithm $\sigma$ versus logarithm $\tau$ is plotted.

One of the advantages of using the Allan variance analysis for a statistical measure of stability is that an Allan variance has a simple dependence on sampling time interval $\tau$ for common characteristics of fluctuations of noise. For example, when the power law spectral densities of fluctuations of noise are white (i.e., $S_y(f)$ equals $h_0$), flicker (i.e., $S_y(f)$ equals $h_{-1}/f$), or random walk (i.e., $S_y(f)$ equals $h_{-2}/f^2$) in nature, the square root of the corresponding Allan variance $\sigma^2(\tau)$ has sampling time interval $\tau$ dependences of $\tau^{-1/2}$, $\tau^0$, and $\tau^{1/2}$, respectively [9], as illustrated in Fig. 9.

### *B. Measurement Techniques for Estimating the Stability of an Individual Noise Source*

When one uses a measurement setup such as a switching radiometer where the measurement system is inherently stable, the technique described as follows is attractive for measurements of the stability of an individual noise source. This type of radiometer samples power from one noise source and then from the

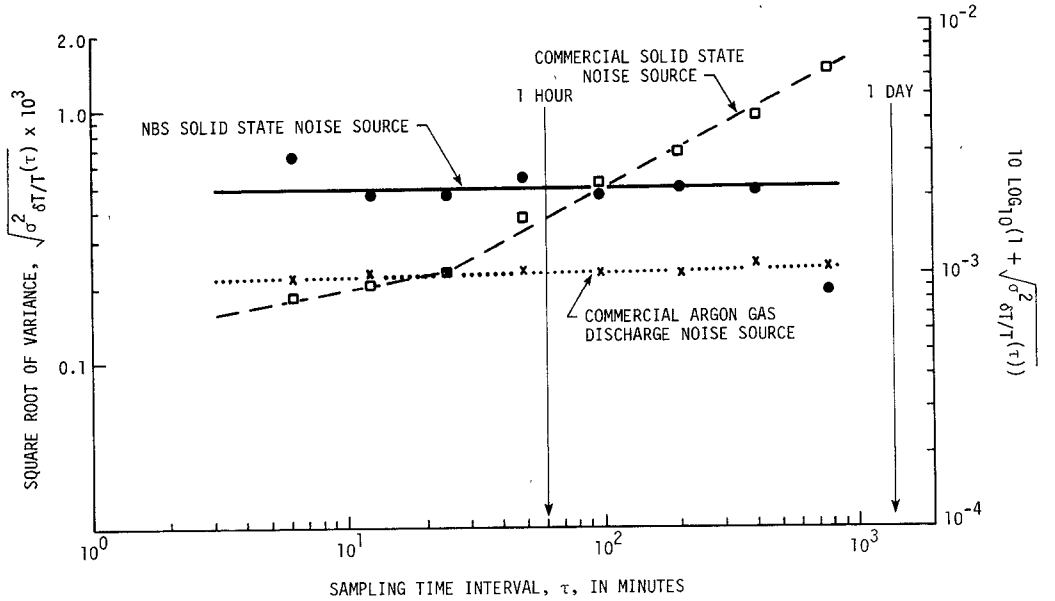


Fig. 10. The square root of Allan variances for fluctuations of noise intensity of noise sources as a function of sampling time interval $\tau$.

other by switching repetitively from one to the other. The switching speed of this switching radiometer is typically 30 Hz. A null balance is usually achieved by adjustment to make the average noise output power from the two noise sources identical. From these two reasons, the measurement system is inherently stable and does not significantly affect the measurement of stability of a noise source.

Using the switching radiometer, the stability of fluctuations of noise intensity from a noise source can be measured by comparing its output with that of the other noise source. The resultant instability includes only the instability of the noise source under consideration as well as that of the reference noise source. The separation of instabilities due to these two noise sources is quite simple. We use three independent noise sources and measure Allan variance of one noise source with respect to the other. Then, for three independent noise sources, we have

$$\sigma_{a,b}^2(\tau) = \tfrac{1}{2}\sigma_a^2(\tau) + \tfrac{1}{2}\sigma_b^2(\tau) + \frac{1}{2M}\sum_{k=1}^{M}(\Delta y_{a,k}\Delta y_{b,k}) \quad (8)$$

where $\Delta y_k$ equals $y_{k+1} - y_k$, the difference between adjacent noise measurement, and $M$ is the number of differences. Similarly,

$$\sigma_{b,c}^2(\tau) = \tfrac{1}{2}\sigma_b^2(\tau) + \tfrac{1}{2}\sigma_c^2(\tau) + \frac{1}{2M}\sum_{k=1}^{M}(\Delta y_{b,k}\Delta y_{c,k}) \quad (9)$$

$$\sigma_{c,a}^2(\tau) = \tfrac{1}{2}\sigma_c^2(\tau) + \tfrac{1}{2}\sigma_a^2(\tau) + \frac{1}{2M}\sum_{k=1}^{M}(\Delta y_{c,k}\Delta y_{a,k}). \quad (10)$$

The cross-product term goes to zero as the number of measurements increases, provided noise sources are independent of each other. Equations (8)–(10) can be solved for an individual Allan variance. For example,

$$\sigma_a^2(\tau) = \sigma_{a,b}^2(\tau) + \sigma_{c,a}^2(\tau) - \sigma_{b,c}^2(\tau) - \frac{1}{2M}\sum_{k=1}^{M}(\Delta y_{a,k}\Delta y_{b,k} + \Delta y_{c,k}\Delta y_{a,k} - \Delta y_{b,k}\Delta y_{c,k}). \quad (11)$$

This technique is used to estimate the stability of fluctuations of noise intensity from individual noise sources, and the experimental results are given in the next section.

## VI. Experimental Results

The NBS solid-state noise source shown in Figs. 6 and 7 is used for the experiments of a statistical stability measure at 3 GHz. The effective noise temperature from this solid-state noise source is typically 290 000 K, and a corresponding excess noise ratio (ENR) is about 30 dB.

Fig. 10 shows the results of the Allan variance analysis for the NBS solid-state noise source. For a one-day sampling time interval the square root of the Allan variance $\sigma$ of $\delta T/T$, where $T$ is the output radiation noise temperature from the NBS solid-state noise source, is 0.0005. This value can be expressed in decibels as $10 \log_{10}(1 + \sigma_{\delta T/T}) = 0.002$ dB. Since the Allan variance is independent of sampling time interval $\tau$, the fluctuations of the output noise from this solid-state noise source behave as a flicker noise process.

To compare the stability of this solid-state noise source with that of a typical commercial solid-state noise source, the square root of the Allan variance of a typical commercial solid-state noise source is also shown in Fig. 10. The fluctuations of the output noise from the commercial solid-state noise source behave as a random walk noise process, since the square root of the Allan variance increases linearly with the square root of sampling time interval $\tau$. For a one-day sampling time interval the square root of the Allan variance of $\delta T/T$, where $T$ is the output radiation noise temperature from this solid-state noise source, is about 0.0018. This value corresponds to 0.008 dB. For comparison purposes, the results of the Allan variance of a typical commerical argon gas-discharge noise source are also shown in Fig. 10. For a one-day sampling time interval the square root of the Allan variance of $\delta T/T$, where $T$ is the output radiation noise temperature from this commercial argon gas-discharge noise source, is about 0.0002. This value corresponds to about 0.001 dB. The stability of the commercial argon gas discharge noise source is found to be very good.

## VII. Conclusion

This short paper describes the modifications made on a typical commercial solid-state noise source in order to improve its long-term stability. The modifications made are 1) heat sinking of the silicon avalanche noise diode, 2) proper dc RF decoupling,

and 3) impedance matching. It is found that the fluctuations of the output noise from this NBS solid-state noise source behave as a flicker noise process, and the square root of the variance of its noise output for one-day sampling time is 0.002 dB. In contrast, the fluctuations of the output noise from the typical commercial solid-state noise source behave as a random walk noise process, and the square root of the variances for its output noise for a one-day sampling time interval is about 0.008 dB. Thus the stability of the NBS solid-state noise source is improved significantly over that of typical commercial solid-state noise sources.

## References


[1] M. Kanda, "A measure for the stability of solid state noise sources," *1975 IEEE-MTT-S International Microwave Symposium Digest*, pp. 315–317, Palo Alto, CA, May 1975.
[2] M. Kanda, "A statistical measure for the stability of solid state noise sources," to be published.
[3] M. E. Hines, "Noise theory for the Read type avalanche diode," *IEEE Trans. Electron Devices*, vol. ED-13, no. 1, pp. 158–163, Jan. 1966.
[4] R. H. Haitz, "Noise of a self-sustaining avalanche discharge in silicon: Studies at microwave frequencies," *J. Appl. Phys.*, vol. 39, no. 7, pp. 3379–3384, June 1968.
[5] W. Shockley, "Problems related to p-n junctions in silicon," *Solid-State Electronics*, vol. 2, no. 1, pp. 35–67, 1961.
[6] For example, J. L. Moll, *Physics of Semiconductors*. New York: McGraw-Hill, 1964.
[7] D. W. Allan, "Statistics of atomic frequency standards," *Proc. IEEE*, vol. 54, no. 2, pp. 221–230, Feb. 1966.
[8] J. A. Barnes *et al.*, "Characterization of frequency stability," *IEEE Trans. Instrum. and Meas.*, vol. IM-20, no. 2, pp. 105–120, May 1971.
[9] J. H. Shoaf, D. Halford, and A. S. Risley, "Frequency stability specification and measurement: High frequency and microwave signals," NBS Technical Note 632, Jan. 1973.


# A New 34-GHz 3.5-mm Low-Cost Utility Coaxial Connector Featuring Low Leakage, Low Standing-Wave Ratio, and Long Life


STEPHEN F. ADAM, SENIOR MEMBER, IEEE,
GEORGE R. KIRKPATRICK,
NORBERT J. SLADEK, MEMBER, IEEE, AND
SAVERIO T. BRUNO, MEMBER, IEEE



***Abstract*—A utility 3.5-mm connector was designed to cover frequencies above 18 GHz in coaxial transmission lines. The superior cost/performance characteristics of this new connector are presented.**


## Introduction

During the late 1950's to early 1960's, the 7-mm coaxial transmission lines with their standard type N connectors were only used to 10 or 12 GHz. With the advent of the precision 7-mm sexless connectors during the first half of the 1960's, the APC-7 and the Precifix A connectors, the frequency range was extended to 18 GHz, which is the practical limit for 7-mm transmission lines. Concurrently, the type N connector went through a redesign phase to cover the same frequency range as the sexless 7-mm connectors. The ever-expanding use of these frequency ranges with requirements of broader bandwidths and new frequency allocations assigned in the U.S. by the Federal Communications Commission and in Europe and other parts of the world by their appropriate agencies, made it quite necessary to extend the useful coaxial instrumentation beyond 18 GHz. For many narrow-band applications, waveguides were already used, but allocations in some cases assigned bands on overlapping band edges.


Manuscript received May 17, 1976; revised August 10, 1976.


S. F. Adam and G. R. Kirkpatrick are with the Stanford Park Division, Hewlett Packard Company, Palo Alto, CA 94304.
N. J. Sladek and S. T. Bruno are with the RF Division, Bunker Ramo, Danbury, CT 06810.


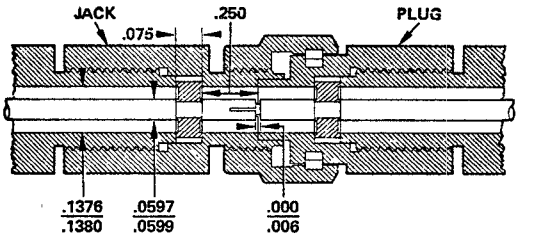


Fig. 1. Cross section of the connectors mated and as assembled on to center and outer conductors.

In the mid 1960's the U.S. Department of Commerce established the Joint Industry Research Committee for the Standardization of Miniature Precision Coaxial Connectors (JIRC/SMPCC). The result of that effort yielded a voluntary product standard in 1972. The air transmission line size was reduced to 3.5 mm to extend the mode-free operation of that line to 36 GHz. A hermaphroditic connector was also proposed, which has been available for years now, and was submitted for standardization to the International Electrotechnical Commission through Technical Committee 46D. These connectors perform quite well; however, due to their high precision, their price tag prohibits them from gaining acceptance for wide usage as a utility connector. The need was clear to design a utility 3.5-mm high-performance low-cost coaxial connector.

Many mechanical properties were considered in the design of this connector (Fig. 1). An objective was to build on experience gained from the use of other RF connectors. An example, the mating surface of the outer conductor on the male connector has a wall thickness of 0.020 in. This relatively thick wall will withstand high contact force insuring good connector repeatability, long life, and low leakage.

The recessed bead has several advantages. The impedance of the transmission line at the connector interface is controlled by only two parameters, that is, the diameters of the center and outer conductors. A sufficiently large spacing between the beads of the connector mated pair was chosen to allow resonance-free operation to 34 GHz. Any higher order modes that may be generated at the transmission lines support (bead) will die out rapidly, and not cause a resonance problem [1]. With air as the interface dielectric there are none of the plastic-filled connector problems such as, 1) an air gap length that is hard to control and can change with temperature, and 2) a line impedance that also depends on the plastic's dielectric constant and dimensions. The additional benefits to the user are that the line impedance can be established by two simple physical measurements and that the performance of any mated pair of these connectors will be very similar.

The material used for center and outer conductors is gold-plated BeCu. This material is used to assure the highest contact pressure and electrical conductivity and is a nonferromagnetic material. Long wear, low loss, and low leakage as well as less susceptibility to damage are the results of using this tough material.

Table I shows the dimensions of an SMA connector outer conductor detail with its tolerances. Minimum and maximum areas of outer conductor contact surfaces are calculated. Maximum allowable compressive loads are calculated from yield strengths taken from available reference data showing stainless steel being inferior to half and full hard BeCu. Furthermore, thread load was calculated using SMA connector specifications, which indicates approximately a 165-lb load applied by